Supporting Information

Photocatalytic Reactive Oxygen Species Generation Activity of TiO_2 Improved by The Modification of Persistent Free Radicals

Jianli Liu,[a] Guohui Dong,*[,a] Jun Jing,[a] Shuyun Zhang,[a] Yu Huang,[b] and Wingkei Ho[c]

[a] School of Environmental Science and Engineering, Shaanxi University of Science and Technology, Xi'an 710021, China

[b] Key Laboratory of Aerosol Chemistry and Physics, Institute of Earth Environment, Chinese Academy of Sciences, Xi'an 710061, China

[c] Department of Science and Environmental Studies and Centre for Education in Environmental Sustainability, The Education University of Hong Kong, Tai Po, N.T. Hong Kong, PR China

*Corresponding author. Phone: +86-029-86132765.

E-mail: dongguohui@sust.edu.cn

S1. Results and Discussion

S1.1 The detail analysis of XRD patterns: To study the crystal structure of different samples, the X-ray diffraction (XRD) patterns of each sample were analyzed. It can be seen from Figure 1a, all the samples display the same XRD peaks (2θ) at 25.16, 37.77, 47.84, 54.01, 55.07, 62.87, 68.90, 70.40 and 75.06°, which corresponds to the characteristic peaks (101), (103), (004), (112), (200), (105), (211), (204), (116), (220), (215), and (224) of anatase phases (JCPDS 71-1166). With the ageing time increase, the different peaks of TiO_2 become wider and wider, indicating the long ageing time can help decrease the grain size of TiO_2 sample.

S1.2 The detail analysis of XPS spectra: To further clear the compositions of different samples, the high resolution elements XPS spectra were analyzed. Figure 2c shows the high resolution Ti 2p XPS spectra of different samples, the Ti 2p XPS spectra of all samples only have two peaks at around 458.3 and 463.9 eV. These two peaks could be ascribed to the Ti $2p_{3/2}$ and Ti $2p_{1/2}$ of Ti(IV), suggesting Ti(III) is not present in all TiO_2 samples. The high resolution C 1s XPS spectra (Figure 2a) of all samples have three peaks at around 284.6, 285.92, and 288.95 eV. According to previous reports, the main peak at 284.6 eV is attributed to the C-C bond with sp^2 orbital, and the peaks at 285.92 and 288.95 eV are assigned to the C-O and COO bonds. These high resolution elements XPS spectra results confirm that the presence of organics on the surface of resulted samples. O 1s XPS spectra of different samples have significant difference. As shown in Figure 2b, the O 1s peaks can be fitted with three peaks at 529.5, 531.1 and 533.2 eV for all samples. These three peaks are related to lattice oxygen of TiO_2, surface -OH, and adsorbed H_2O respectively.

S1.3 The formation process analysis of organics: TiO_2 precursor (TBOT) has lots of organic ligands (OL), which can be hydrolyzed into butanol, $Ti(OH)_4$, or incomplete hydrolysate (Such as OL-$Ti(OH)_3$) in the aging process. There is no stirring in the aging process. Therefore, the longer aging time will cause the more complete hydrolysis. Meanwhile, hydrolysates could aggregate with each other and form the gel micelle. In the calcining process, the remanent organic ligands would decompose and form Ti-O-CH_2-CH_3, while the butanol would decompose to -CH_2-CH_2-OH and -CH_2-CH_3. Then, HO-CH_2-CH_2- would be oxidized to -CH_2-COOH, which is a strong electron withdrawing group. This electron withdrawing group could bond with the O terminal of TiO_2 and form Ti-•O-CH_2-COOH.

S1.4 The detail analysis of $\bullet O_2^-$ spectra: $\bullet O_2^-$ was measured through the electron paramagnetic resonance (EPR) spectroscopy. As shown in Figure S2, no any EPR signal can be found in the EPR spectra of three samples in the dark condition. After 5 min of light illumination, three samples clearly display the characteristic EPR signal of $\bullet O_2^-$. Meanwhile, the intensity of $\bullet O_2^-$ signal in 8h-TiO_2 and 12h-TiO_2 samples are more than that in 4h-TiO_2 sample.

S1.5 Active species scavenger experiment: Since •OH can be produced through both the oxidation of hole and the reduction of electron. KI was chosen as hole scavenger to clear the approach of •OH generation over different samples. As shown in Figure 7e, the photocatalytic •OH production ability of different samples are inhibited clearly by the addition of KI. The inhibition rates of 4h-TiO_2, 8h-TiO_2, and 12h-TiO_2 are 28%, 61%, and 54%, respectively. This result implies that EPFRs may also help holes to take part in the •OH production. As we known, the higher surface area may absorb more light or adsorb more electrolyte ions. Meanwhile, the more lights or electrolyte ions will produce the higher photocurrent densities. However, in our experiment systems, the sizes of different working electrodes (different samples) are the same. Therefore, the surface area can be excluded from the influence factors.

S1.6 Electrochemical property: Electrochemical impedance spectra (EIS) measurements were carried out to study the internal charge transfer. Figure 6h presents the Nyquist impedance results for Xh-TiO_2 under dark. The smaller radius of the arc implies the higher efficiency of charge transfer. Therefore, 8h-TiO_2 have the best electronic transfer properties among three samples. The photocurrent densities were detected under visible irradiation to investigate the photoelectric conversion properties of different samples. As shown in Figure 6g, all the samples

have rapid photo-response. Among different samples, 8h-TiO_2 shows the highest photocurrent, suggesting that 8h-TiO_2 possesses better photoelectric conversion property than other samples.

S1.7 The detail analysis of Kelvin probe force microscopy (KPFM): Kelvin probe force microscopy (KPFM) was employed to test the surface potential of 8h-TiO_2 sample. As shown in Figure S4, the nano-tubes exists on the surface of 8h-TiO_2, which consists the EPFRs. Importantly, electric potential difference can be evidenced between EPFRs and the bulk of TiO_2, confirming the existence of built-in electric field.

S1.8 Photocatalytic NO removal experiments: Photocatalytic NO removal experiments were carried out in a continuous flow quartz reactor (High = 10 cm, Radius = 5 cm). TiO_2 sample was made into a membrane in a sample dish (High = 1.5 cm, Radius = 3 cm). This sample dish was then put into the middle of the reactor. A 300W XE lamp with certain wavelength filter (420 nm and 550 nm) was selected as the light source. The NO source employed the air stream mixed with 600 ppb of NO gas. This air stream was allowed continuous flowing through the reactor with the flow rate of 1 L min^{-1}. The NO concentration during reactions was continuously monitored by a NOx analyzer (Thermo Scientific, 42i).

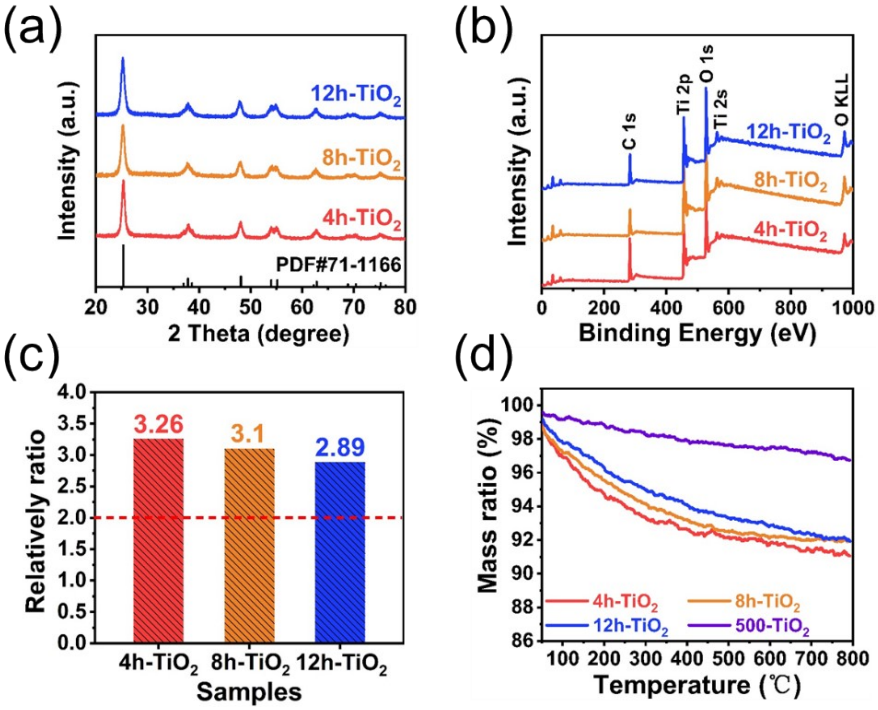

Figure S1. XRD patterns of Xh-TiO_2 samples (a); XPS survey spectra of Xh-TiO_2 samples (b); O/Ti ratio of Xh-TiO_2 samples (c); TGA curves of different samples (d).

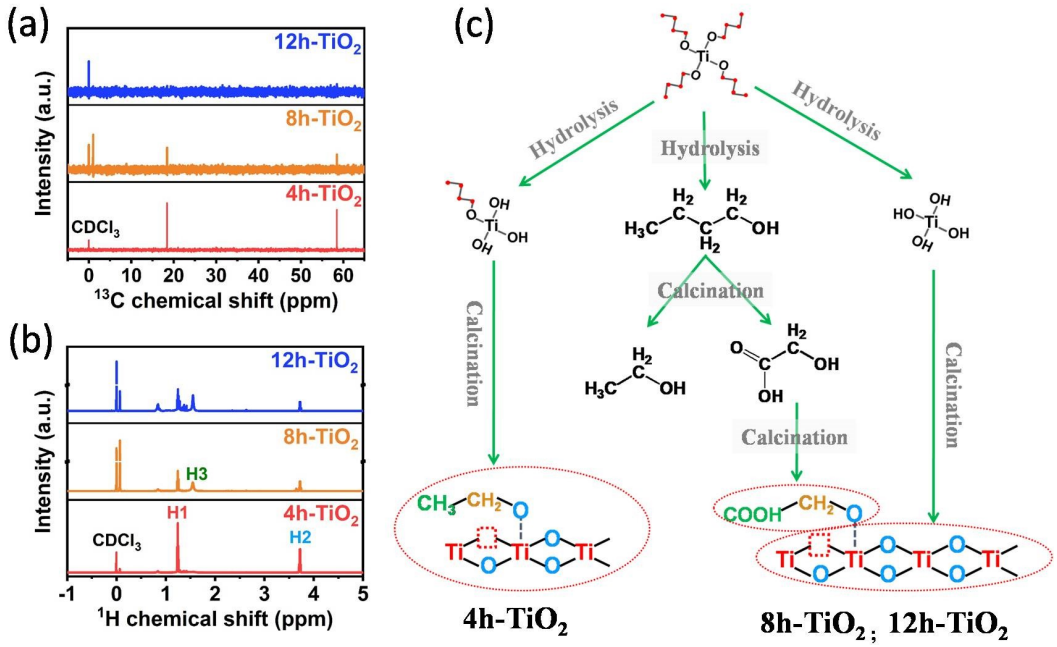

Figure S2. ^{13}C NMR spectra (a) and ^{1}H NMR spectra (b) of Xh-TiO_2 acquired with 600 MHz spectrometer; Schematic illustration of organics generation (c).

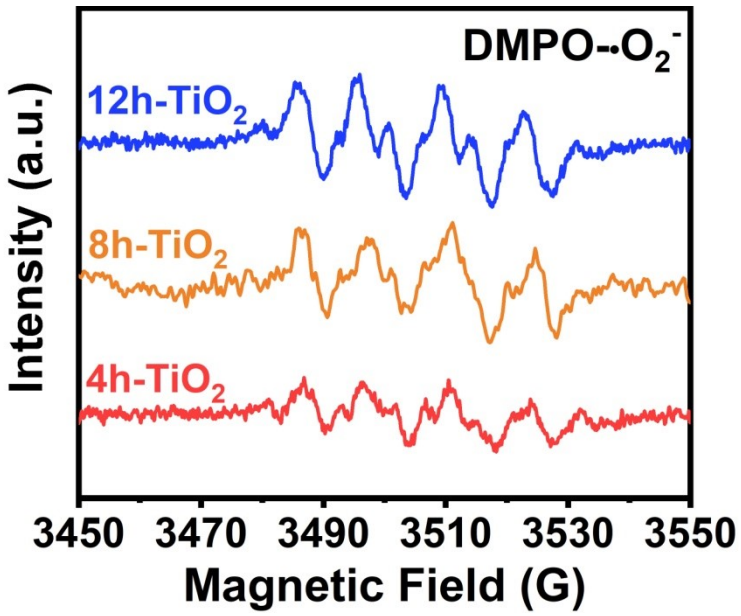

Figure S3. ESR spectra of the DMPO-•O_2^- adducts recorded with as-prepared TiO_2. under simulated sunlight irradiation.

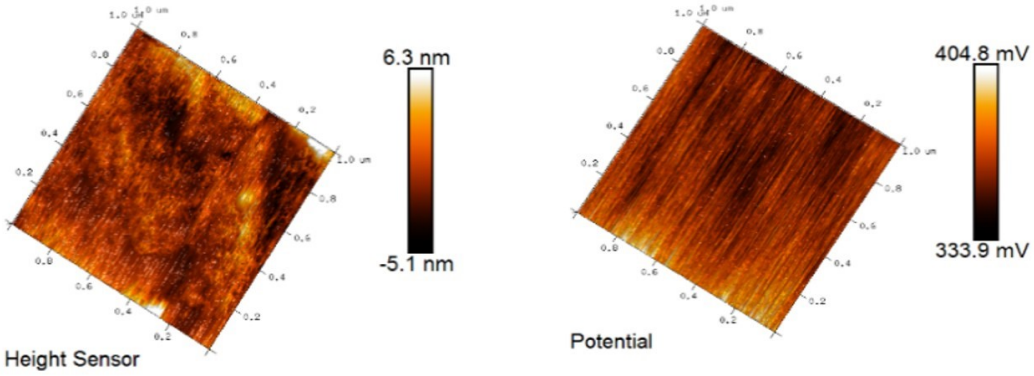

Figure S4. KPFM images of 8h-TiO_2.

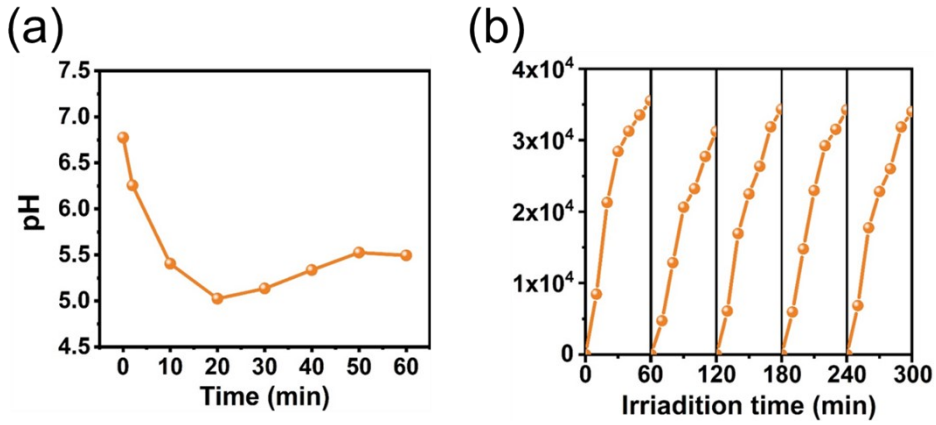

Figure S5. (a) pH variation of solution during photocatalytic H_2O_2 production; (b) Recycling test of 8h-TiO_2 for photocatalytic •OH production.

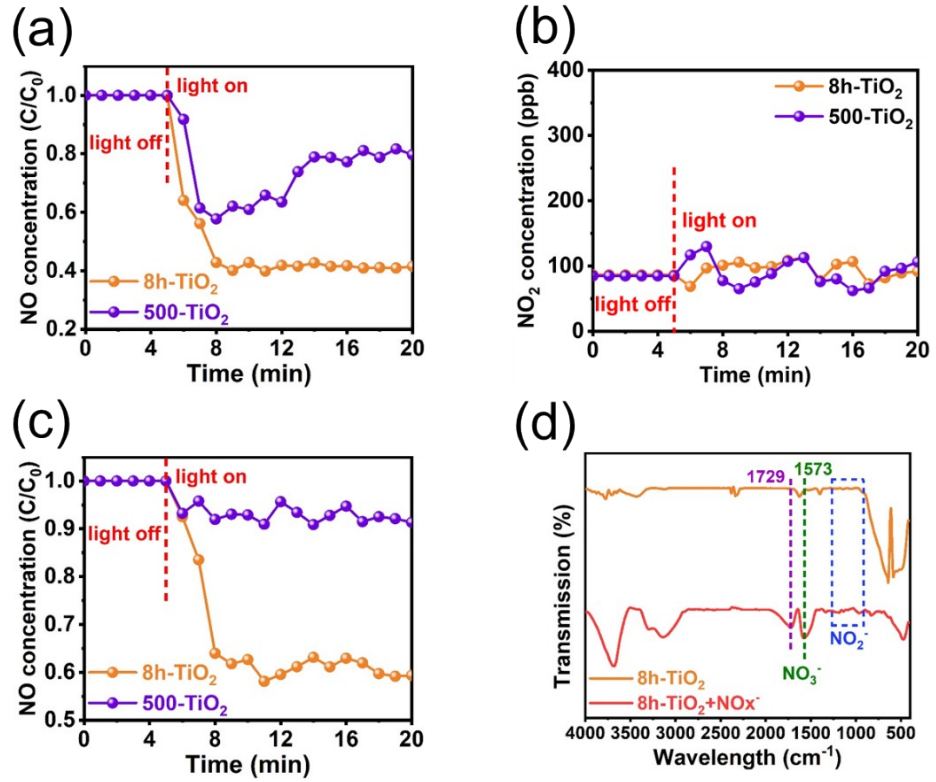

Figure S6. (a) The change of NO concentration (C/C_0) over 8h-TiO_2 and 500-TiO_2 under visible irradiation; (b) NO_2 concentration changes with increase of irradiation time over 8h-TiO_2 and 500-TiO_2; (c) The NO removal over 8h-TiO_2 and 500-TiO_2 samples under green light irradiation (λ=550 nm); (d) FTIR spectra of 8h-TiO_2 before and after NO removal experiment.